Targeting breast and pancreatic cancer metastasis using a dual-cadherin antibody

Douglas S. Micalizzi[a,b], Dante Che[a], Benjamin T. Nicholson[a], Jon F. Edd[a,c], Niyati Desai[a], Evan R. Lang[a], Mehmet Toner[c,d], Shyamala Maheswaran[a,d], David T. Ting[a,b,1] 🄳, and Daniel A. Haber[a,b,e,1]

The successful application of antibody-based therapeutics in either primary or metastatic cancer depends upon the selection of rare cell surface epitopes that distinguish cancer cells from surrounding normal epithelial cells. By contrast, as circulating tumor cells (CTCs) transit through the bloodstream, they are surrounded by hematopoietic cells with dramatically distinct cell surface proteins, greatly expanding the number of targetable epitopes. Here, we show that an antibody (23C6) against cadherin proteins effectively suppresses blood-borne metastasis in mouse isogenic and xenograft models of triple negative breast and pancreatic cancers. The 23C6 antibody is remarkable in that it recognizes both the epithelial E-cadherin (CDH1) and mesenchymal OB-cadherin (CDH11), thus overcoming considerable heterogeneity across tumor cells. Despite its efficacy against single cells in circulation, the antibody does not suppress primary tumor formation, nor does it elicit detectable toxicity in normal epithelial organs, where cadherins may be engaged within intercellular junctions and hence inaccessible for antibody binding. Antibody-mediated suppression of metastasis is comparable in matched immunocompetent and immunodeficient mouse models. Together, these studies raise the possibility of antibody targeting CTCs within the vasculature, thereby suppressing blood-borne metastasis.

cancer metastasis | cadherins | circulating tumor cells | antibody therapeutics | breast cancer

Antibody-based therapeutics are poised to transform the treatment of cancer, combining precise targeting of a cell surface epitope on cancer cells with the delivery of a payload or recruitment of cytotoxic immune cells to enhance elimination of neoplastic cells (1, 2). In breast cancer the antibody trastuzumab, targeting the growth factor receptor encoded by the *HER2* oncogene, substantially improves patient outcomes in metastatic *HER2*-amplified breast cancer, and it suppresses cancer recurrence in women with localized disease thereby enhancing cure rates (3, 4). Trastuzumab is thought to exert its antitumor effects in genetically defined breast cancer subsets through suppression of a receptor tyrosine kinase pathway critical for cancer cell proliferation and survival, as well as through the induction of antibody-dependent cellular cytotoxicity (ADCC) mediated by activation of cytotoxic T cells. The success of an antibody targeting HER2 has led to the development of multiple trastuzumab-based antibody-drug conjugates (ADC), including TDM-1 (5) and Trastuzumab deruxtecan (6), which carry a chemotherapeutic payload that is released within cellular endosomes following internalization of the antibody (7). The landscape of potential targets for anti-cancer antibody development has recently been expanded with the Food and Drug Administration (FDA) approval for triple negative breast cancer of the ADC Sacituzumab govitecan (8), which targets a cell surface protein, Trop2, without oncogenic activity. Thus, successful targeting of breast and other cancers may hinge on the selection of robust target epitopes, that deliver toxins or mediate immune activation to achieve clinical responses.

Cadherin proteins form adherens junctions through homotypic interactions at the cell surface between adjacent cells (9). This calcium-dependent adhesive property is essential to the normal role of cadherins in maintaining epithelial structures. The cadherins are frequently dysregulated in cancer, which is characterized by a less stationary and more migratory cell phenotype (10). Plasticity between epithelial phenotypes is associated with distinct cadherin gene family members: epithelial-mesenchymal transition (EMT) is accompanied by down-regulation of epithelial E-cadherin (CDH1) and up-regulation of mesenchymal cadherins including *N*-cadherin (CDH2) and osteoblast cadherin (OB-cadherin or cadherin-11 or CDH11) (11). These expression changes are mediated in part by master transcriptional regulators of EMT (SNAIL, SLUG, and TWIST) (12), and the migratory mesenchymal phenotype may be reversed in the process of mesenchymal-epithelial transition (MET), as disseminated cancer cells establish proliferative metastases (13). The dynamic expression of cadherins may limit the effectiveness

of highly specific antibodies targeting a single gene product, favoring antibodies that recognize multiple related cadherins. Moreover, cadherins that are tightly bound in adherens junctions within normal epithelial structures may be shielded from antibody exposure, whereas invasive tumor cells with disorganized epithelial architecture may have exposed cadherin proteins on their cell surface that may be targeted by therapeutic antibodies.

Here we describe a dual anti-cadherin antibody that binds to a homologous region within the cadherin family of proteins and impairs metastatic outgrowth in murine syngeneic and xenograft breast cancer models and in a xenograft pancreatic cancer model. Despite its binding to both human and murine cadherin proteins, treatment of mice with the antibody does not demonstrate evidence of toxicity to normal epithelial organs. These studies suggest potential applications of a cadherin-based antibody therapeutic as a method to target epithelial cancer cells.

Results

Heterogeneity of Cadherin Expression and Binding by the 23C6 Antibody. To investigate the cadherin proteins as potential targets for the rational design of an antibody therapeutic, we examined the landscape of cadherin expression in both primary cancers and in circulating tumor cells (CTCs) from patients with metastatic cancer. RNA expression of the cadherin family in the TCGA dataset across different histological types of primary cancers shows high levels of expression with the exception of B-cell lymphoma, representing a hematological malignancy lacking epithelial junctions (Fig. 1A). E-cadherin (CDH1) is most highly expressed across epithelial cancers (97.2% of samples express >5 fragments per kilobase of exon per million (FPKM) at the RNA level across 16 epithelial cancers), but significant heterogeneity across other cadherin family members is evident, with N-cadherin (CDH2) (38.4%), P-cadherin (CDH3) (60.4%), and OB-cadherin (CDH11) (38.9%) as the dominant family members expressed in epithelial cancers.

We have previously shown that CTCs exhibit heterogeneity in their expression of epithelial and mesenchymal marker proteins, including the cadherin proteins, both at baseline and during the course of therapeutic interventions (14). To further characterize the heterogeneity of cadherin expression, we analyzed single cell RNA-Seq of CTCs isolated from patients with metastatic hormone receptor positive (HR$^+$) breast cancer. Compared with primary tumors, CTCs demonstrate considerably higher variability in cadherin expression: CDH1 is again the predominant cadherin in breast CTCs, but with only 32.1% of single CTCs expressing at >5 reads per million (RPM) (34/106 CTCs from 32 patients) (Fig. 1B). Combining all cadherins with >5 RPM achieves coverage of 61.3% of CTCs. In contrast, the expression of the cadherin family in hematopoietic cells is minimal compared with expression in epithelial tissues (*SI Appendix*, Fig. S1). Together, this analysis suggests that targeting multiple cadherin family members would have the advantage of addressing heterogeneity in expression of individual gene family members across CTCs. This concept is further supported by the known dynamics of cadherin expression in breast cancer, including the frequent loss of CDH1 expression in lobular carcinomas of the breast (15), and EMT-associated plasticity with transient suppression of CDH1 associated with cancer invasion (16).

The mouse monoclonal antibody 23C6 was initially developed against the extracellular domain of CDH11 (17). Upon sequencing its variable domains and modeling the antibody's potential docking site on CDH11, we identified two potential binding sites within the extracellular domain (Fig. 1C), both of

which are highly conserved between CDH11 and CDH1 (58.5% and 42.9% amino acid homology for potential binding sites 1 and 2, respectively) (Fig. 1D). The two proposed binding sites have contacts across all three heavy chain complementary-determining regions (CDRs) of the 23C6 antibody, however proposed binding site 1 is predicted to have contacts with the light chain CDR2 while proposed binding site 2 is predicted to have contacts across all three light-chain CDRs. Indeed, Western blot analysis reveals strong reactivity with recombinant human CDH11, as well as human and murine CDH1, that was not observed using an independent CDH11 antibody (3H10) (Fig. 1E), consistent with the recognition of a conserved region. We observed lesser reactivity with human CDH2 (*SI Appendix*, Fig. S2A). The reactivity of the 23C6 antibody with CDH1 was verified by ectopic expression of murine or human CDH1 in L-M cells (18) that lack endogenous cadherin expression (*SI Appendix*, Fig. S2B). To confirm the dual specificity of the 23C6 antibody, we generated shCDH11 knockdown cell lines in MDA-MB-231 cells that do not express CDH1 (*SI Appendix*, Fig. S3) and observed a loss of signal detecting CDH11 by Western blot (*SI Appendix*, Fig. S4 A and B). Furthermore, we knocked down expression of CDH1 in PDAC9 cells, which predominantly express CDH1, and demonstrate a shift in the reactivity with the 23C6 antibody by flow cytometry (*SI Appendix*, Figs. S3 and S4 C–E); however, we note moderate maintained reactivity that could be from known CDH11 expression in this cell line. To determine the spectrum of breast cancers with reactivity to the 23C6 antibody, we stained a tumor array of 96 breast cancers consisting of HR$^+$, HER2$^+$, and triple negative (TNBC) breast cancers. Immunohistochemical staining demonstrates the expected cell membrane staining pattern, with 79% of all breast cancers having strong staining of tumor cells, including 88% of HR$^+$ and 60% of TNBC subtypes of breast cancers (Fig. 1 F and G).

Given that the 23C6 antibody recognizes CDH1 and CDH11, we evaluated the expression of these two cadherin family members at the RNA and protein level across different cancer types. With the exception of hematologic malignancies, virtually all cancers express detectable RNA and protein for at least one of these cadherin genes (Fig. 1H and *SI Appendix*, Fig. S5). Similar findings are observed among primary cancer-derived cell lines (19), where 624/921 (67.8%) express at least one of these two cadherins (>5 RPM) (*SI Appendix*, Fig. S6). Finally, across metastatic breast cancer patients, 47.1% (8/17) have a combined average expression of CDH1 and CDH11 in their CTCs greater than >20 RPM; given heterogeneity among CTCs, 41.2% (7/17) of patients have more than one third of their CTCs expressing such levels of CDH1 or CDH11 (Fig. 1I).

Suppression of Metastasis by 23C6 Antibody in a Mouse Breast Tumor Model. To assess the potential anti-metastatic activity of the 23C6 antibody, we first selected murine TNBC-related 4T1 breast cancer cells, whose tumorigenicity in syngeneic mice provides a model for ADCC and immune related functions. Following orthotopic mammary gland inoculation of 4T1 cells, we treated mice with twice weekly with the antibody (5 mg/kg intraperitoneal injection) starting on the day of inoculation (Fig. 2A). Primary tumor growth was not significantly different between placebo and 23C6-treated mice (Fig. 2B). Tumors were resected after 20 d (median size 200 mm^3) followed by continued antibody treatment, and the metastatic burden in the lungs was assessed after 36 d. Antibody-treated mice showed a dramatic decrease in metastatic burden, both in the number and size of metastatic deposits (tumor percentage
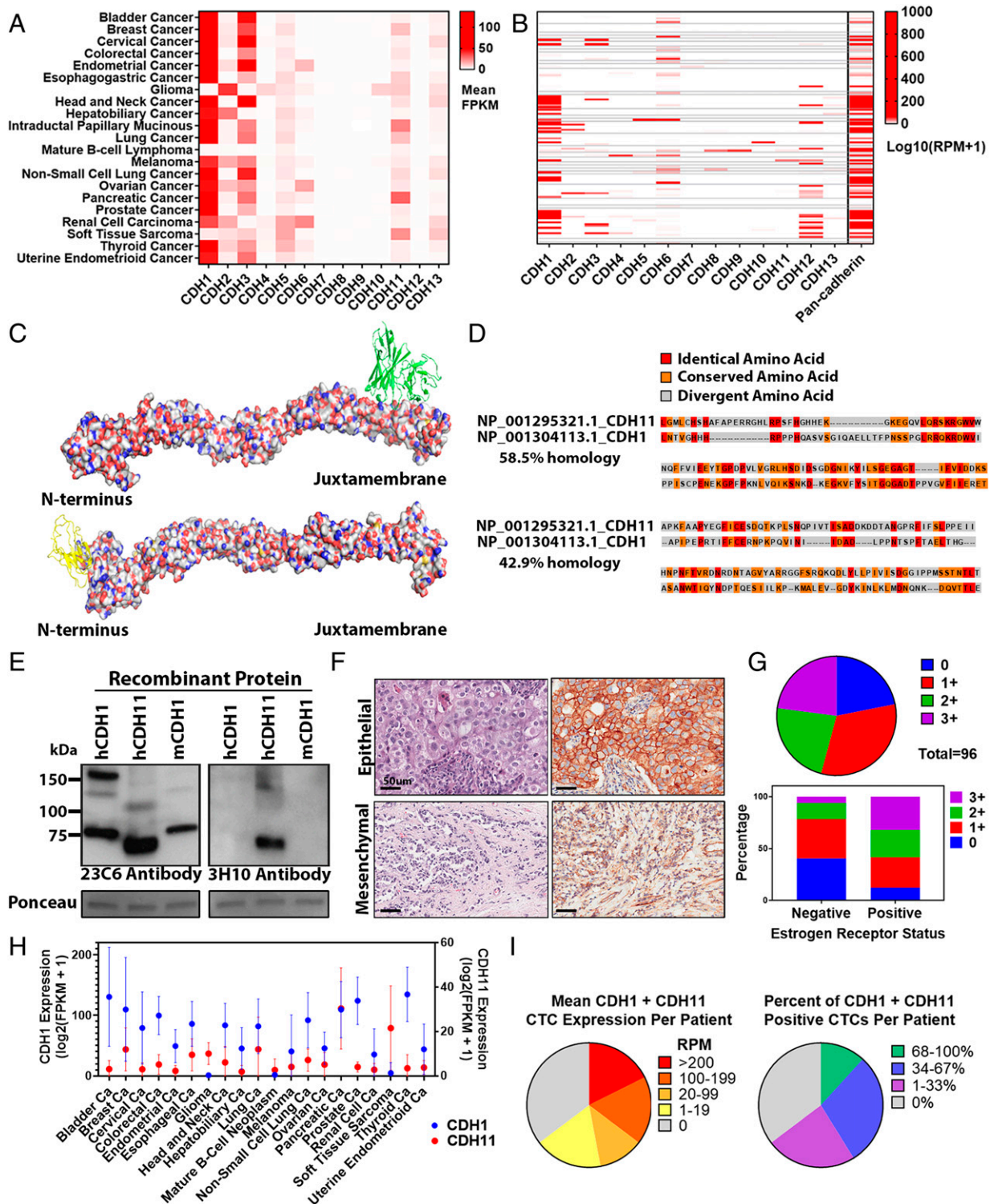
Fig. 1. (*A*) Analysis of RNA-Seq data from TCGA Pan-cancer analysis with mean value for the FPKM for each cancer type and each cadherin family member. (*B*) RNA-seq from CTCs enriched from whole blood with the iChip microfluidic device and isolated as single cells. Expression values represent log10(RPM+1). Gray horizontal lines demarcate individual patients. (*C*) Three-dimensional modeling of the top two docking sites of the antigen binding region (ribbon model) of the 23C6 antibody on the extracellular domain of CDH11 (space filling model). *Upper:* Binding free energy difference (ΔE) = −46.4 and *Lower* model with ΔE = −32.6. (*D*) Protein sequence alignment using Clustal omega of the two docking sites of the 23C6 antibody on CDH11 compared to the protein sequences for CDH1. Colors represent amino acid properties: Red, identical amino acids; orange, conserved amino acids with combined strongly and weakly similar properties. (*E*) Western blot analysis of recombinant purified hCDH1, hCDH11 and mCDH1 proteins detected with 23C6 antibody or a CDH11 specific antibody 3H10. "h" indicates human and "m" indicated murine. Loading control with Ponceau staining. High molecular weight bands likely represent aggregation of the highly purified proteins. (*F*) H&E staining (*Left*) and 23C6 immunohistochemical staining (*Right*) of representative sections of two different tumors from a breast cancer tumor array. Upper right scored as 3+ for tumor cell membrane staining. Lower right scored as 1+ for tumor cell membrane staining. (*G*) Distribution (*Upper*) and breakdown in ER positive and negative tumors (*Lower*) of membranous staining intensity on a scale of 0 (no staining) to 3+ (intense staining). (*H*) Analysis of RNA-Seq data from TCGA Pan-cancer analysis of whole genomes with mean value for the FPKM for CDH1 and CDH11. Error bars represent SD. (*I*) RNA-seq from single cell CTCs enriched from whole blood from metastatic breast cancer patients. (*Left*) Proportion of patients with average expression of the combined sum of CDH1 and CDH11 in the indicated ranges. (*Right*) Proportion of CTCs with >5 RPM expression of CDH1 and CDH11 within individual patients.
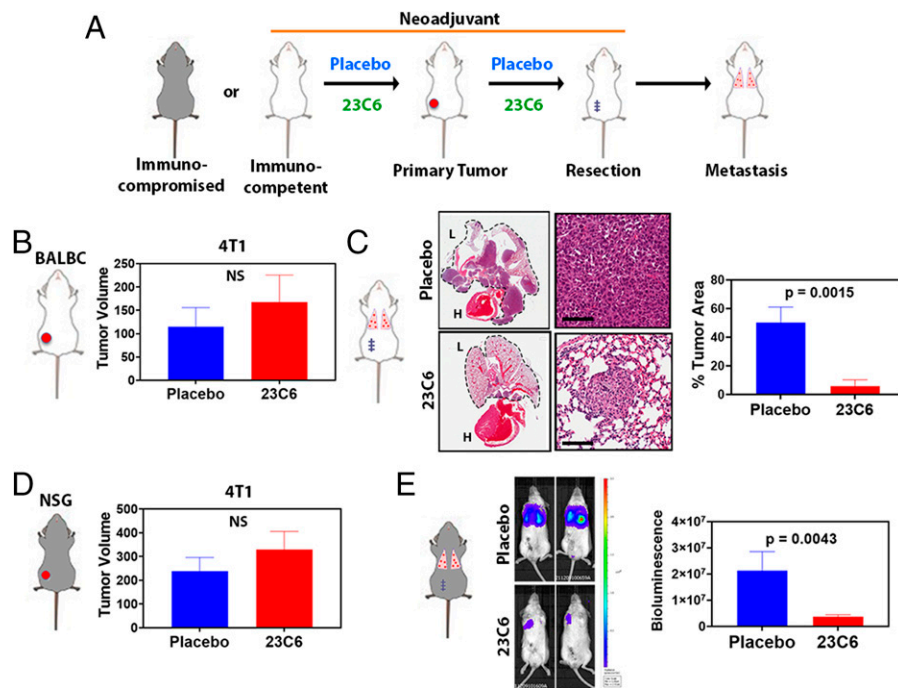
Fig. 2. (A) Schema for the mouse models of neoadjuvant placebo or 23C6 treatment. (B) Tumor volume measurements of 4T1 orthotopic mammary gland tumors in BALBC immunocompetent mice treated with placebo or 23C6 antibody at day 20 prior to resection (n = 5 to 6 mice per treatment arm). (C) Representative H&E sections of lung and heart whole mount (lungs outlined with dashed line) in placebo and 23C6 treated mice. High magnification section of representative lung metastases. Right panel with quantified percentage tumor area (n = 5 to 6 mice per treatment arm). (D) Tumor volume measurements of 4T1 orthotopic mammary gland tumors in NSG immunocompromised mice treated with placebo or 23C6 antibody at day 20 prior to resection (n = 5 to 6 mice per treatment arm). (E) Representative whole body bioluminescent images in placebo and 23C6 treated mice. (Right) Quantification of total body bioluminescent imaging (n = 5 to 6 mice per treatment arm). Error bars represent SEM. P values calculated by unpaired Mann–Whitney tests.

of 50.3 vs. 5.8%; P = 0.0015) suggesting that 23C6 impairs metastasis in this model (Fig. 2C).

To test whether the effect of the 23C6 antibody is dependent on an intact immune system, we repeated the 4T1 tumorigenesis experiment in NSG immunocompromised mice. Compared with the immunocompetent model, 4T1 cells generated larger primary tumors in NSG mice, and again 23C6 antibody treatment did not impact primary tumor cell growth (Fig. 2D). However, as in the immunocompetent model, there was a significant decrease in lung metastatic burden in mice treated with 23C6 antibody (Fig. 2E). Thus, antibody treatment effectively decreases metastasis, independent of immune cell activation.

Efficacy of 23C6 Antibody in Human Tumor Xenografts. We extended studies of 23C6 antibody efficacy across different human xenograft models in NSG immunodeficient mice. The MDA-MB-231 cell line is an aggressive and metastasis-prone model of the TNBC subtype of breast cancer, lacking expression of CDH1, but expressing CDH11 (*SI Appendix,* Fig. S3). Orthotopic mammary tumor formation by these cells was not significantly affected by 23C6 treatment (Fig. 3A), but administration of antibody for 39 d before and 4 d after resection of the primary tumor was sufficient to significantly suppress metastatic burden in both lungs and liver (Fig. 3 B and C). In these cells, shRNA-mediated knockdown using two independent constructs (68% and 83% knockdown) impaired metastatic growth without affecting primary tumor formation (*SI Appendix,* Fig. S7). These observations suggest that CDH11-dependent functions may be disrupted either by antibody binding or genetic knockdown, with comparable consequences for metastasis in this model.

To investigate whether the 23C6 antibody directly affects cancer cells, we treated the MDA-MB-231 cells grown in vitro with the 23C6 antibody and assessed viability, growth, and invasiveness. Treatment with the 23C6 antibody did not affect cell viability, even at high doses, and it did not impair cell proliferation (*SI Appendix,* Fig. S8 A and B). However, 23C6 antibody treatment decreased MDA-MB-231 cell migration through a Boyden chamber at high and low doses of the 23C6 antibody, suggesting that impaired motility may contribute to the observed anti-metastatic activity (*SI Appendix,* Fig. S8 C).

Like the TNBC subtype of breast cancer, pancreatic ductal adenocarcinoma (PDAC) represents a highly aggressive malignancy with limited treatment options and with heterogeneous expression of diverse cadherin proteins. We tested the 23C6 antibody in a patient-derived pancreatic cell line, PDAC9, that spontaneously develops metastases after subcutaneous injection. Western blot analysis demonstrates protein expression of CDH1 and reactivity with the 23C6 antibody (*SI Appendix,* Fig. S3). Primary tumor formation by PDAC9 cells in NSG mice was not significantly reduced by continuous treatment with the 23C6 antibody (Fig. 3D). However, after resection of the primary tumor, 23C6 antibody-treated mice had a 25-fold reduction in metastatic burden measured via total body luminescence (P = 0.01) (Fig. 3E). Importantly, in this highly vascular invasive tumor model we were able to enumerate the number of CTCs in the blood at the terminal timepoint. Antibody-treated mice demonstrated a 100-fold reduction in the number of CTCs (median 238 vs. 4 CTC per milliliter of blood, P = 0.01) (Fig. 3F). Together, these xenograft studies (44 mice across three different models) demonstrate the efficacy of a dual cadherin targeting antibody, across different tumor types, in suppressing blood-borne metastasis by epithelial cancers, even in immunosuppressed mouse models.

While antibodies may suppress proliferation and induce ADCC, their conjugation with cytotoxic drugs to create ADCs has the potential to enhance their cytotoxicity. We therefore conjugated 23C6 antibody to SN-38, the highly potent metabolite of the
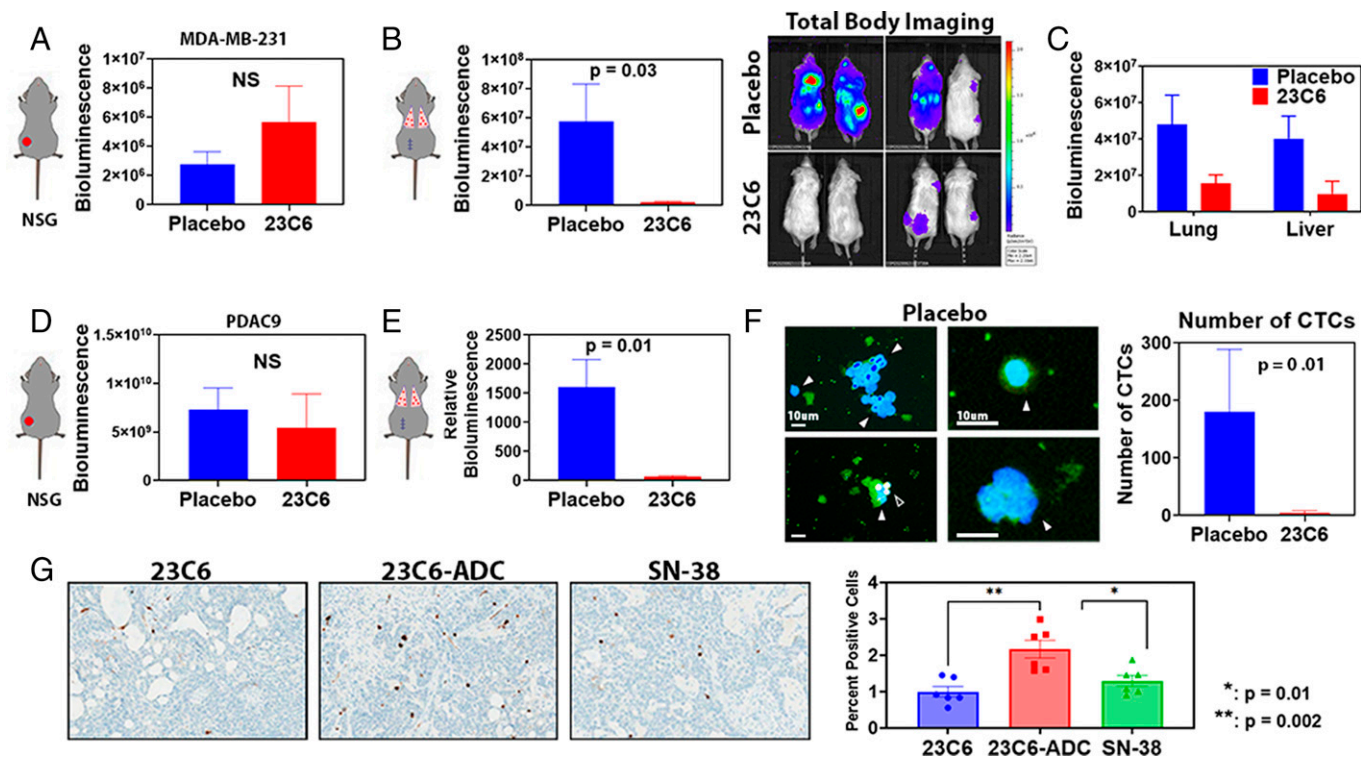
Fig. 3. (*A*) Primary tumor bioluminescence measurement of MDA-MB-231 orthotopic mammary gland tumors in NSG immunocompromised mice treated with placebo or 23C6 antibody at day 36 prior to resection (*n* = 5 mice per treatment arm). (*B*, *Left*) Quantification of total body bioluminescent imaging of MDA-MB-231 cells in placebo and 23C6 treated mice. *P* values calculated by unpaired Mann–Whitney Tests. (*Right*) Representative whole body bioluminescent images (*n* = 5 mice per treatment arm). (*C*) Quantification of ex vivo bioluminescent signal of the lung and liver from mice treated with placebo or 23C6 after dissection on day 74. (*D*) Primary tumor bioluminescence measurement of PDAC9 subcutaneous flank tumors in NSG immunocompromised mice treated with placebo or 23C6 antibody at day 32 prior to resection (*n* = 4 mice per treatment arm). (*E*) Quantification of total body bioluminescent imaging of PDAC9 cells in placebo and 23C6 treated mice. *P* values calculated by unpaired Mann–Whitney tests. (*F*) Immunofluorescent imaging of single and clustered CTCs stained with DAPI (blue), human specific HLA antibody (green) or mouse specific CD45 (red). White arrowhead indicates CTCs while black arrowhead indicated CD45 positive cells. (*Right*) Quantification of the number of CTCs in PDAC9 injected, placebo, and 23C6 treated mice. *P* values calculated by two tailed unpaired *t* test (*n* = 4 mice per treatment arm). (*G*) Representative immunohistochemical staining of cleaved caspase-3 indicating apoptotic cells in primary tumors derived from PDAC9 cells in mice treated with naked 23C6, 23C6 conjugated to SN38 or an equimolar SN-38. Quantification of as the percentage of cleaved caspase-3 positive cells in right panel. *P* values calculated by two tailed unpaired *t* test. (*n* = 3 mice per treatment arm) Error bars represent SEM.

Topoisomerase I inhibitor irinotecan (20). Successful conjugation was confirmed by HPLC with only 8% estimated aggregation (*SI Appendix*, Fig. S9) and the drug:antibody ratio was calculated to be 1.84. Sufficient quantities of the 23C6-ADC were produced for a single administration in mice with an established PDAC9-derived tumor. Histological analysis at 8 d posttreatment demonstrated an increased fraction of apoptotic tumor cells (cleaved caspase-3) in 23C6-ADC treated mice (2.2%), compared with mice receiving either equimolar naked 23C6 antibody (1%, *P* = 0.002) or equimolar SN-38 drug alone (1.3%, *P* = 0.019) (Fig. 3*G*).

Lack of Toxicity to Normal Epithelial Tissues by Antibody 23C6. Cadherin expression is ubiquitous across normal epithelial tissues, raising the significant concern that therapeutic targeting of these proteins may induce antibody-mediated inflammation and toxicity in normal organs. The 23C6 antibody recognizes recombinant murine CDH1 protein (Fig. 1*E*), a cross-reactivity that is supported by its effectiveness against mouse 4T1 tumor cells. To examine the effect of antibody treatment on normal mouse organs, we treated immunocompetent BALBC mice with 23C6 antibody (5 mg/kg twice per week for 32 d), followed by histological analysis of multiple organs. Histological appearance of multiple tissues, including kidney, liver, colon, and muscle, was indistinguishable between antibody- and placebo- treated mice, with no evidence of increased cell death (cleaved caspase-3), disruption of epithelial borders or blood

vessels (CD34) or immune cell infiltration (CD45) (Fig. 4 *A–C* and *SI Appendix*, Fig. S10). At 32 d, antibody-treated mice were not externally distinguishable from controls, maintaining identical levels of activity and mass (mean mass 20.7 g for placebo vs. 20.6 g for 23C6 treated mice), organ mass on necropsy (Fig. 4 *D* and *E*), white blood cell count and hemoglobin levels in the blood (*SI Appendix*, Fig. S11). Thus, despite their ubiquitous expression in normal tissues, targeting cadherins CDH1 and CDH11 does not result in evident toxicity.

Reactivity of the 23C6 Antibody Across Cancer Histologies. To determine the spectrum of cancers with potential reactivity for the 23C6 antibody, we stained a tumor tissue array with 124 individual samples derived from 18 different human cancers. All solid tumor types, with the exception of medulloblastoma, testicular, and bladder cancers, had more than 50% of samples positive for membranous staining using the 23C6 antibody (Fig. 5 *A* and *B*). Breast cancers, across all histological subtypes, show the highest proportion of tumors with strong staining for 23C6. However, other prevalent cancer types including pancreatic cancer, colon cancers, and lung cancers frequently showed high reactivity with the 23C6 antibody, expanding the potential activity of the 23C6 antibody to other common cancers.

Discussion

Antibody-based therapeutics for cancer combine the targeting of specific cell surface epitopes, with the ability to conjugate
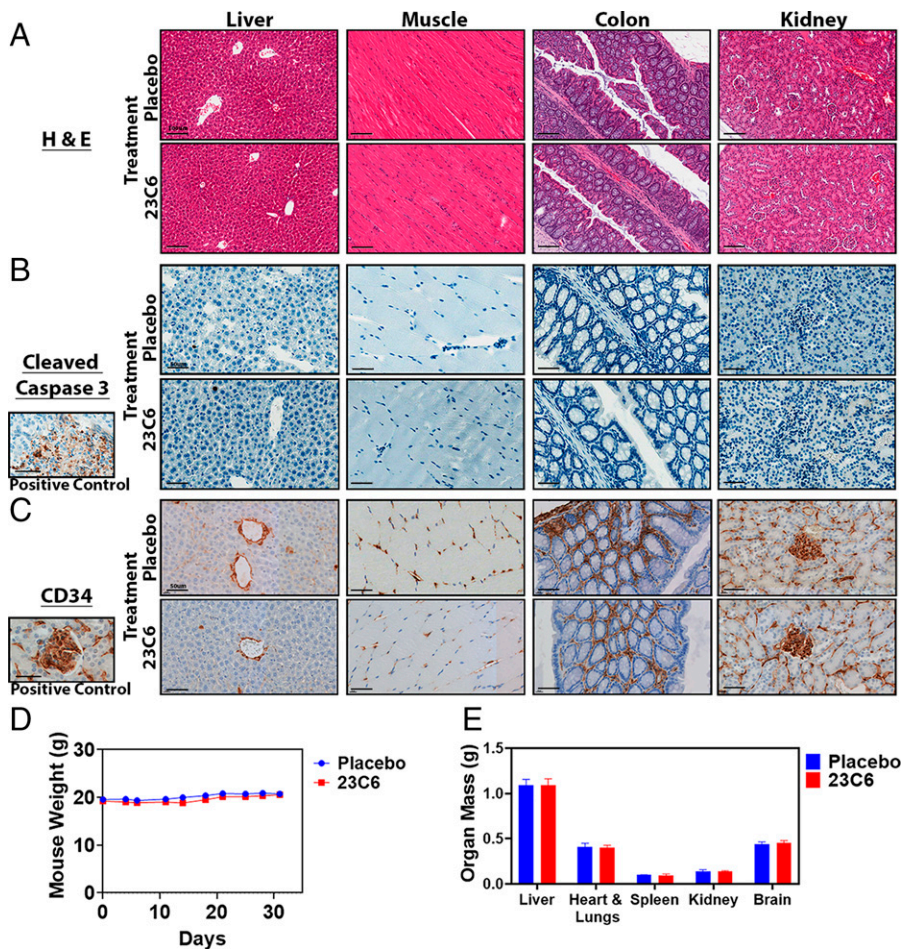
Fig. 4. (*A*) H&E staining. (*B*) cleaved caspase 3 and (*C*) CD34 immunohistochemical staining of sections of organs derived from BALBC mice treated with placebo or 23C6. Positive control for cleaved caspase 3 and CD34 in *Inset*. (*D*) Measurement of mouse masses over time with treatment of a placebo or 23C6 antibody. (*E*) Measurement of organ weights after treatment with placebo or 23C6 for 31 d upon necropsy. (*n* = 5 mice per treatment arm). Error bars represent SEM.

such antibodies to a cytotoxic drug or other bioactive molecule, thereby potentially enhancing both efficacy and specificity. Current clinically approved antibody therapies target oncogene-encoded drivers of cancer cell proliferation, such as HER2 in breast cancer (4) and epidermal growth factor receptor (EGFR) in lung and colorectal cancer (21); specific lineage markers of cell differentiation, including CD38 in multiple myeloma (22) and CD20 in lymphoma (23), and molecules that are critical to the vascular and immune tumor microenvironment, notably vascular endothelial growth factor (VEGF) to suppress angio-genesis (24) and PD1/PDL1 to activate T-cell immune responses (25). In this context, the recent clinical approval for the TNBC subtype of breast cancer of sacituzumab govitecan, an ADC targeting the cell surface glycoprotein Trophoblast antigen-2 (Trop2), is of particular interest (8). Trop2 is widely expressed in normal tissues as well as malignancies, where it plays a role in calcium-dependent signaling that has not been specifically linked to tumorigenesis or malignant cell prolifera-tion (26). Its striking clinical success suggests an expanded list of cell surface epitopes that may be relevant in cancer therapy, highlighting the importance of carefully selected antibody tar-gets, irrespective of a functional role in tumorigenesis.

Here, we have shown that an antibody targeting multiple cadherins, expressed in both epithelial (CDH1) and mesenchy-mal (CDH11) cell types does not appear to be toxic to normal tissues, and does not suppress primary tumor formation, but effectively suppresses the blood-borne metastatic spread to lungs and other distant organs (Fig. 5*C*). We hypothesize that

the lack of normal organ toxicity reflects the fact that cadherins are physiological components of intercellular adherens junc-tions, hence the epitope recognized by the 23C6 antibody may not be accessible in normal tissues. A similar rationale may explain the absence of effect on the formation of primary tumors within tissues. In the bloodstream, however, individual or clustered cancer cells and cell surface molecules are readily accessible for antibody binding, and indeed, we find that 23C6 antibody suppresses metastatic dissemination. Supporting this hypothesis, treatment of nonpermeabilized MCF7 mammary carcinoma cells growing in a monolayer using 23C6 antibody detected by immunofluorescence shows markedly reduced staining in confluent areas, compared with strong staining in cells with exposed borders of reduced 23C6 staining and less confluent areas with enhanced staining (*SI Appendix*, Fig. S12).

CTCs are derived from primary tumors or from metastatic deposits, as cancer cells acquire access to the vasculature and disseminate through the bloodstream to distant organs (27). Most CTCs die in the bloodstream, from loss of intercellular contacts, circulatory shear stress or high oxygen tensions, but a subset remain viable and give rise to new metastatic lesions. Targeting CTC-mediated metastasis in the bloodstream pro-vides a remarkable opportunity for epitope selection: while can-cer cells lodged within epithelial organs may not harbor many distinguishing cell surface markers, cancer cells in the circula-tion are surrounded by hematopoietic cells that share very few markers of epithelial lineage, thus providing for considerable degree of selectivity. Nonetheless, single cell RNA seq studies
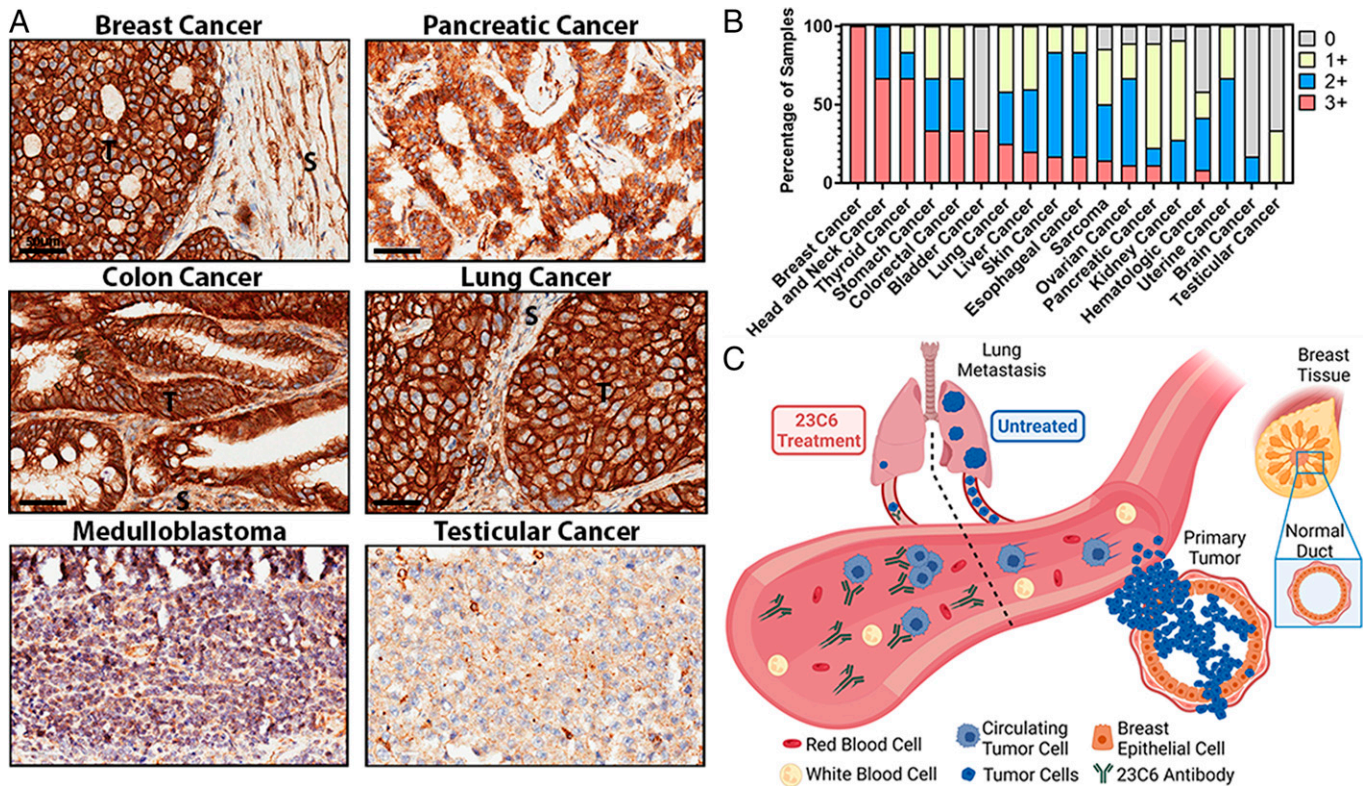
Fig. 5. (*A*) Representative immunohistochemical staining with 23C6 of breast, pancreatic, colon and lung cancer, medulloblastoma, and testicular cancer sections; T = tumor, S = stroma. (*B*) Quantification of intensity of membrane staining of tumor sections from a tumor array on a scale of 0 (no staining) to 3+ (intense staining). (*C*) Model of 23C6 antimetastatic activity. Primary tumor cells access the circulation as CTCs and then exit the vasculature at a distant organ site as precursors of metastases. The 23C6 antibody decreases the number of CTCs in circulation which then leads to decreased metastatic dissemination without affecting primary tumor growth or normal organs and tissues of the body.

have demonstrated extensive heterogeneity among CTC subpopulations that include cadherin switching with CDH1 switching to other cadherins in the context of EMT (14, 28, 29), necessitating careful selection of broad coverage across CTCs, while also minimizing the potential toxicity to normal tissues.

Further studies will be required to distinguish antibody-mediated effects as CTCs transit through the bloodstream versus subsequent effects on tumor cell extravasation or early metastatic initiation. In the pancreatic tumor cell model tested, antibody treatment led to a profound decline in CTC numbers within the vascular space, consistent with an effect on either CTC shedding or survival in the bloodstream. While our studies have focused on cadherin proteins as abundant and targetable cell surface markers irrespective of their functional properties, their cellular roles may also contribute and prevent their down-regulation which would cause loss of antibody efficacy. CDH11 has been shown to be necessary for metastatic spread in a mouse model of breast cancer (30), a finding supported by our CDH11-shRNA knockdown studies. A CDH11 targeted antibody has also been reported to decrease tumor growth in mouse models of breast and other cancers (31, 32). CDH1 has also been implicated as a contributor to metastatic spread in breast cancer (33). In pancreatic cancer, genetically engineered mouse models have demonstrated an importance of CDH1 localization on EMT plasticity and mode of cellular invasion (34). While these studies have used mouse models, therapeutic anti-CDH11 antibodies are currently in clinical trials for treatment of rheumatoid arthritis, suggesting a favorable safety profile for targeting this cadherin (35). Thus, our studies raise the possibility of antibody targeting of multiple cadherins to suppress the heterogeneous paths of cancer metastasis.

While metastasis is the major source of lethality in solid tumors, there are no currently approved therapies that specifically target the metastatic process or the subset of invasive cells responsible for cancer spread. This reflects both the technological challenge of detecting and targeting cancer cells in the bloodstream, as well as the clinical conundrum of how best to deploy such anti-metastatic strategies. As novel bioengineering and molecular technologies enable reliable isolation of CTCs and characterization of their expression profiles at the single cell level, specific vulnerabilities may emerge for therapeutic applications. These may include intracellular pathways that contribute to CTC survival in the high oxygen environment of the vasculature (36, 37) or expression of cell surface markers that are lacking in surrounding normal blood cells. In addition to the uniqueness of their cell surface markers, CTCs in the bloodstream are in direct contact with immune cells and with the reticulo-endothelial system of the spleen and liver, which may serve to increase clearance of antibody coated CTCs. Modification of antibodies to enhance their half-life in the bloodstream may further improve their therapeutic index when targeting cell surface epitopes shared by normal tissues.

From a clinical standpoint, there are two critical stages of cancer treatment where a specific anti-metastatic strategy may be deployed to complement standard therapeutic approaches. First, in the preoperative (neo-adjuvant) and postoperative (adjuvant) setting, where chemotherapy is routinely administered in high-risk tumors, including breast cancers, both to increase the likelihood of complete surgical resection, and to eradicate possible distant micrometastatic disease. Metastatic spread may be initiated long before a primary tumor is first diagnosed, but some clinical data have also suggested that physical manipulation of

tumors at the time of surgical resection may release cancer cells into the circulation (38). In such cases, presurgical administration of anti-metastatic therapies might reduce the likelihood of distant spread associated with surgical resection. Second, the current revolution in highly effective targeted and immunologic cancer therapies has revealed a clinical window in which oligometastatic disease can be treated before the development of widespread metastases. In such cases, administration of anti-metastatic therapies at the first sign of disease recurrence, in combination with standard anti-cancer therapies, may reduce the further metastatic spread of an early recurrence. Together, these conceptual scenarios may provide initial strategies for future testing of metastasis suppressors. The efficacy of a multicadherin antibody in targeting CTC-dependent blood-borne metastasis in preclinical mouse models raises the possibility of such anti-metastatic therapies.

Materials and Methods

Antibody Generation. The 23C6 antibody was generated as previously described (17). The hybridoma derived 23C6 clone was a generous gift from Dr. Michael Brenner (Brigham and Women's Hospital, Boston MA). The hybridoma derived 23C6 clone was expanded for bioreactor production, purified and concentrated (Antibody Solutions). Conjugation of the 23C6 antibody was performed using PerKit Antibody SN38 Conjugation Kit (Cell Mosaic). Briefly, 1 mg of 23Cg was prepared and then added to O-succinyl SN38 NHS ester and incubated at room temperature overnight according to the manufacturer's recommendation. The conjugate was then purified using a desalting column washed and eluted. To confirm successful conjugation, hydrophobic interaction chromatography (HIC) high performance liquid chromatography (HPLC) was used. Analysis of the antibody conjugate aggregation was performed using size exclusion chromatography (SEC) HPLC. To determine the concentration of the SN38-labeled 23C6, UV/Vis spectrophotometry with absorbance at 380 nm and 280 nm was performed and a drug to antibody ratio (DAR) was calculated. The DAR was ~1.84 and the aggregation was ~8%.

Antibody Binding Modeling. Next generation sequencing was used to determine the RNA sequence of the V-region of the heavy and light chains for 23C6 from the hybridoma. To predict the antibody structure, NovaFold application software (DNASTAR Inc.) was used which searches the input sequence against thousands of nonredundant protein antibody structures from Protein Data Bank and finds the best templates for the chain. An energy minimization calculation was performed to construct the final predicted structure of the antibody. For CDH11, the protein amino acid sequence was modeled using I-TASSER (39, 40) multiple template threading methodology in the NovaFold application software. Protein-protein docking analysis was performed using an algorithm based on SwarmDock which makes docking predictions based on the particle swarm optimization (41).

Western Blot Analysis. Western blot analysis was performed on whole cell extracts prepared with radioimmunoprecipitation assay (RIPA) buffer. Proteins were separated on 4 to 15% polyacrylamide gradient-SDS gels (Bio-Rad) and transferred onto nitrocellulose membrane (Invitrogen). Immunoblots were visualized with Enhanced Chemiluminescence (Perkin-Elmer). Primary antibodies were used against E-cadherin (1:5,000; BDBiosciences Clone 36), N-cadherin (1:500; EBiosciences Clone 8C11) and GAPDH (1:2,000; Millipore ABS16). 23C6 was also used as a primary antibody for Western blot analysis (1:250). Recombinant protein obtained as follows: human CDH1 (R&D Systems 8505-EC-050), murine CDH1 (R&D Systems 8875-EC-050), human CDH2 (R&D Systems 1388NC050) and human CDH11 (Elabscience #PKSH032136).

Quantitative Real-Time PCR. RNA was isolated using RNeasy Mini Kits (Qiagen). RNA was reverse-transcribed using SuperScript III First Strand Synthesis Supermix (Invitrogen). TaqMan probe and primer sets for CDH11 and GAPDH were used.

Histology and Immunohistochemistry. Tumors and multiple organs were fixed in 10% formalin overnight, then preserved in 70% ethanol. The tissue was embedded in paraffin and cut in 5-μm sections. For histologic analysis, sections

were stained with hematoxylin and eosin or immunohistochemical staining was performed. Tissues were permeabilized, and antigen retrieval was performed in 1× citrate buffer (pH 6) for 15 min. Slides were washed and blocked for 30 min with 5% goat serum. Sections were incubated with primary antibodies against 23C6 (1:250), CD45 (1:2,000; Abcam ab281586), CD34 (1:2,000; Abcam ab81289), Cleaved caspase-3 (1:1,000; Cell Signaling Technology 9664S) for 1 h at room temperature. Slides were incubated with horseradish peroxidase (HRP) anti-rabbit antibody (DAKO) for 30 min. After washing with phosphate-buffered saline (PBS), the sections were incubated in 3,3′-diaminobenzidine (Vector Laboratories) for 10 min. Cells were counterstained with Gill's #2 hematoxylin for 10 to 15 s. Stained tissue sections were digitized using the Aperio CSO (Leica Biosystems) or Vectra Polaris (Perkin-Elmer). Tumor foci in the lungs were quantified by Halo Imaging software (Indica Labs). Tissue and tumor arrays were obtained from US Biomax and prepared and stained as described above. The following tissue arrays were used: multicancer tumor array #BC001134b, breast cancer specific tumor array #BC081116, and normal tissue array #BN1021.

Cell Culture. Cell lines were routinely checked for mycoplasma (MycoAlert, Lonza), and were obtained from ATCC. 4T1, MDA-MB-231, MCF7, and L-M cells were grown as recommended by ATCC. PDAC9 were grown as previously described (42). Viability assays were performed at 48 h after treatment with varying concentration of the 23C6 antibody or PBS control. Viability was determined using Cell Titer Glo reagent (Promega). Proliferation assays were performed by treating MDA-MB-231 cells with a single dose of 23C6 antibody or PBS control and timepoints as indicated, where the relative cell number was determined with the Cell TiterGlo reagent. For migration assays, the MDA-MB-231 cells were harvested with trypsin, and the cells suspended in serum free media. The cell suspension was added to the upper chamber of a Boyden chamber cell culture plate insert with a gradient generated by adding full serum media in the lower chamber. The cell suspensions were treated with 23C6 or control, and after 48 h, the number of cells migrating through the membrane was determined by crystal violet staining and microscopic imaging with automated counting of individual cells using Image J. For siRNA knockdown, ONTARGETplus siRNA smartpools (Horizon Discovery) were obtained and transfected using Lipofectamine RNAiMax reagent (Invitrogen) and the cells harvested for analysis after 5 d. For flow cytometry, in brief the cells were fixed with 4% PFA, blocked with 5% bovine serum albumin (BSA) in PBS and incubated with the 23C6 antibody at 1:500 followed by anti-mouse IgG-AlexaFluor 555 and then analyzed on BD Fortessa machine. For immunofluorescence staining, MCF7 cells were grown in a monolayer and treated with 23C6 antibody at 1:500 for 1 to 2 h then fixed and permeabilized and incubated with anti-mouse IgG-AlexaFluor 555, Phalloidin-Alexa Fluor-488, and DAPI and mounted and imaged.

Lentivirus Production. HEK293T cells were grown in high-glucose DMEM supplemented with 10% fetal bovine serum and 1% penicillin/streptomycin. Cells were transfected at ~80% confluency with Lipofectamine (Invitrogen). Twenty-four hours after transfection, the media was changed. Virus supernatant was harvested 48 h posttransfection, filtered through a 0.45-μm polyvinylidene fluoride (PVDF) filter.

Lentiviral Transduction. MDA-MB-231 cells were transduced with shCDH11 encoding lentivirus in 6-well plates in 2 mL media supplemented with 6 μg/mL polybrene. Twenty-four hours after infection, media was changed. Seventy-two hours after infection, cells were selected using puromycin (3 μg/mL) for 7 d.

Mouse Experiments. NOD.Cg-Prkdcscid Il2rgtm1Wjl/SzJ (NSG) and BALB/cj mice were obtained from The Jackson Laboratory. 4T1, MDA-MB-231, and PDAC9 cell lines were labeled with GFP-Luciferase for in vivo imaging. Female mice ~6 wk old were injected with 10,000 4T1 cells or 200,000 MDA-MB-231 cells into the fourth mammary gland. For PDAC9, 200,000 cells were injected subcutaneously in the flank. All injections were performed with a 1:1 mixture of growth factor depleted Matrigel. Primary and metastatic growth was measured weekly via in vivo imaging using the IVIS Lumina II (PerkinElmer) following intra-peritoneal injection of D-luciferin (Sigma). For 4T1 injections into BALB/c mice in vivo tumor caliper measurements were used for the primary tumor. At the time of primary tumor resection, the mice were anesthetized with isoflurane and the tumor resected under sterile conditions with the use of electric cautery. Oral analgesics were administered per standard animal protocols with buprenorphine. The mice were monitored two to three times per week. At the terminal

time points, the mice were either injected with D-luciferin for ex vivo organ bioluminescence imaging or blood obtained from cardiac sampling. The mice were treated with twice weekly intraperitoneal injections of placebo (sterile PBS) or 23C6 antibody with 5 mg/kg dosing. For the 23C6-ADC experiment, a PDAC9 derived primary tumor was generated by injection of 500,000 cells subcutaneously in the flank. After primary tumor formation on day 14 postinjection, a single dose of equimolar 23C6, 23C6-SN-38, or SN38 was administered via intraperitoneal injection. The mice were sacrificed after 7 d and the tumor harvested for immunohistochemistry (IHC). For 23C6 toxicity experiments, female BALB/c mice were treated with twice weekly intraperitoneal injections of placebo (sterile PBS) or 23C6 antibody with 5 mg/kg dosing for 31 d. Body weight was monitored twice weekly. At the termination of this experiment, the organs were harvested, weighed, and prepared for IHC. A sample of blood was collected for complete blood count analysis.

CTC Isolation and Identification. On average per mouse, 440 μL of blood was obtained via retro-orbital collection at the terminal timepoint, directly into EDTA, for a final concentration of 5 mM. Tumor-derived cells and cell clusters were then concentrated and separated from white blood cells, red blood cells, platelets, and plasma by size-based sorting using our microfluidic CTC cluster chip, at 10 psi input pressure, as described (43). To improve priming and prevent fouling of microchannel walls by blood components, CTC cluster chips were prefilled with a 0.2% wt/vol solution of an amphiphilic block copolymer (Pluronic F127, Sigma Aldrich) in PBS. After isolation into the same buffer, purified CTCs and CTC clusters were fixed (0.5% PFA, 10 min), plated onto slides using the Shandon EZ megafunnel (Thermo Fisher) and Cytospin cytocentrifuge (2,000 rpm, 5 min), and then processed for automated immunofluorescent imaging. Staining highlighted human HLA (clone W6/32 in Alexa-Fluor 488, *BioLegend*) on CTCs, mouse CD45 (30-F11 clone in AlexaFluor 647, *BioLegend*) and CD16+CD32 (2.4G2 clone in AlexaFluor 647, *LSBio*) on white blood cells, and cell nuclei (DAPI). Slide images were captured and digitized with *Vectra Polaris* multispectral imaging (PerkinElmer). Image analysis was performed with *Halo* imaging software (Akoya Biosciences) to identify potential CTCs and then manually evaluated and enumerated.

Bioinformatic Analysis. For analysis of the TCGA data, RNA-Seq data for the CDH family of genes across cancer types was accessed from cBioPortal. Values representing transcripts per millions were utilized and the mean expression values across each individual cancer type was plotted on a heat map or scatter plot with SD values represented by the error bars. For analysis of single cell RNA-Seq dataset from breast cancer CTCs, the CTCs were isolated, RNA isolated and processing of RNA-Seq data performed as previously described (28). Expression of CDH family of genes was determined as log10(RPM+1) and represented on a heat map grouped by individual patients and individual CTCs. For analysis of CCLE, the dataset was downloaded from (https://sites.broadinstitute.org/ccle/datasets) as RPKM (44). The data were log transformed and plotted on a 3-dimensional axis using OriginLab. For analysis of CDH expression across blood cell types in ProteinAtlas, the data were downloaded from (https://www.proteinatlas.org/about/download) and TPM values plotted on a heat map (45). The proportion of patients with strong to moderate staining for CDH1, CDH2, and CDH11 protein was calculated and plotted. Unless otherwise noted, plots and graphs were generated with GraphPad. Model was generated with BioRender software.

Author affiliations: ᵃMassachusetts General Hospital Cancer Center, Harvard Medical School, Charlestown, MA 02129; ᵇDepartment of Medicine, Massachusetts General Hospital, Harvard Medical School, Boston, MA 02114; ᶜCenter for Bioengineering in Medicine, Massachusetts General Hospital and Harvard Medical School, and Shriners Hospital for Children, Boston, MA 02114; ᵈDepartment of Surgery, Massachusetts General Hospital, Harvard Medical School, Boston, MA 02114; and ᵉHoward Hughes Medical Institute, Chevy Chase, MD 20815

Author contributions: D.S.M., J.F.E., S.M., D.T.T., and D.A.H. designed research; D.S.M., D.C., B.T.N., J.F.E., N.D., and E.R.L. performed research; J.F.E. and M.T. contributed new reagents/analytic tools; D.S.M., M.T., S.M., D.T.T., and D.A.H. analyzed data; and D.S.M., S.M., D.T.T., and D.A.H. wrote the paper.

1. C. H. Chau, P. S. Steeg, W. D. Figg, Antibody-drug conjugates for cancer. *Lancet* **394**, 793–804 (2019).
2. J. Ma *et al.*, Bispecific antibodies: From research to clinical application. *Front. Immunol.* **12**, 626616 (2021).
3. E. H. Romond *et al.*, Trastuzumab plus adjuvant chemotherapy for operable HER2-positive breast cancer. *N. Engl. J. Med.* **353**, 1673–1684 (2005).
4. M. J. Piccart-Gebhart *et al.*; Herceptin Adjuvant (HERA) Trial Study Team, Trastuzumab after adjuvant chemotherapy in HER2-positive breast cancer. *N. Engl. J. Med.* **353**, 1659–1672 (2005).
5. S. Verma *et al.*; EMILIA Study Group, Trastuzumab emtansine for HER2-positive advanced breast cancer. *N. Engl. J. Med.* **367**, 1783–1791 (2012).
6. S. Modi *et al.*; DESTINY-Breast01 Investigators, Trastuzumab deruxtecan in previously treated HER2-positive breast cancer. *N. Engl. J. Med.* **382**, 610–621 (2020).
7. E. G. Kim, K. M. Kim, Strategies and advancement in antibody-drug conjugate optimization for targeted cancer therapeutics. *Biomol. Ther. (Seoul)* **23**, 493–509 (2015).
8. A. Bardia *et al.*; ASCENT Clinical Trial Investigators, Sacituzumab Govitecan in metastatic triple-negative breast cancer. *N. Engl. J. Med.* **384**, 1529–1541 (2021).
9. H. Oda, M. Takeichi, Evolution: Structural and functional diversity of cadherin at the adherens junction. *J. Cell Biol.* **193**, 1137–1146 (2011).
10. U. Bedi, V. K. Mishra, D. Wasilewski, C. Scheel, S. A. Johnsen, Epigenetic plasticity: A central regulator of epithelial-to-mesenchymal transition in cancer. *Oncotarget* **5**, 2016–2029 (2014).
11. M. A. Nieto, R. Y. Huang, R. A. Jackson, J. P. Thiery, Emt: 2016. *Cell* **166**, 21–45 (2016).
12. A. Puisieux, T. Brabletz, J. Caramel, Oncogenic roles of EMT-inducing transcription factors. *Nat. Cell Biol.* **16**, 488–494 (2014).
13. N. P. Gunasinghe, A. Wells, E. W. Thompson, H. J. Hugo, Mesenchymal-epithelial transition (MET) as a mechanism for metastatic colonisation in breast cancer. *Cancer Metastasis Rev.* **31**, 469–478 (2012).
14. M. Yu *et al.*, Circulating breast tumor cells exhibit dynamic changes in epithelial and mesenchymal composition. *Science* **339**, 580–584 (2013).
15. E. Burandt *et al.*, E-Cadherin expression in human tumors: A tissue microarray study on 10,851 tumors. *Biomark. Res.* **9**, 44 (2021).
16. J. P. Thiery, H. Acloque, R. Y. Huang, M. A. Nieto, Epithelial-mesenchymal transitions in development and disease. *Cell* **139**, 871–890 (2009).
17. D. M. Lee *et al.*, Cadherin-11 in synovial lining formation and pathology in arthritis. *Science* **315**, 1006–1010 (2007).
18. H. P. Kiener, C. S. Stipp, P. G. Allen, J. M. Higgins, M. B. Brenner, The cadherin-11 cytoplasmic juxtamembrane domain promotes alpha-catenin turnover at adherens junctions and intercellular motility. *Mol. Biol. Cell* **17**, 2366–2376 (2006).
19. M. Ghandi *et al.*, Next-generation characterization of the Cancer Cell Line Encyclopedia. *Nature* **569**, 503–508 (2019).
20. C. Bailly, Irinotecan: 25 years of cancer treatment. *Pharmacol. Res.* **148**, 104398 (2019).
21. T. S. Mok *et al.*, Gefitinib or carboplatin-paclitaxel in pulmonary adenocarcinoma. *N. Engl. J. Med.* **361**, 947–957 (2009).
22. H. M. Lokhorst *et al.*, Targeting CD38 with daratumumab monotherapy in multiple myeloma. *N. Engl. J. Med.* **373**, 1207–1219 (2015).
23. B. Coiffier *et al.*, CHOP chemotherapy plus rituximab compared with CHOP alone in elderly patients with diffuse large-B-cell lymphoma. *N. Engl. J. Med.* **346**, 235–242 (2002).
24. T. J. Perren *et al.*; ICON7 Investigators, A phase 3 trial of bevacizumab in ovarian cancer. *N. Engl. J. Med.* **365**, 2484–2496 (2011).
25. J. Brahmer *et al.*, Nivolumab versus docetaxel in advanced squamous-cell non-small-cell lung cancer. *N. Engl. J. Med.* **373**, 123–135 (2015).
26. S. Lenárt *et al.*, Trop2: Jack of all trades, master of none. *Cancers (Basel)* **12**, 3328 (2020).
27. D. S. Micalizzi, S. Maheswaran, D. A. Haber, A conduit to metastasis: Circulating tumor cell biology. *Genes Dev.* **31**, 1827–1840 (2017).
28. R. Y. Ebright *et al.*, Deregulation of ribosomal protein expression and translation promotes breast cancer metastasis. *Science* **367**, 1468–1473 (2020).
29. D. T. Ting *et al.*, Single-cell RNA sequencing identifies extracellular matrix gene expression by pancreatic circulating tumor cells. *Cell Rep.* **8**, 1905–1918 (2014).
30. J. H. Chen *et al.*, Monospecific antibody targeting of CDH11 inhibits epithelial-to-mesenchymal transition and represses cancer stem cell-like phenotype by up-regulating miR-335 in metastatic breast cancer, in vitro and in vivo. *BMC Cancer* **19**, 634 (2019).
31. S. Assefnia *et al.*, Cadherin-11 in poor prognosis malignancies and rheumatoid arthritis: Common target, common therapies. *Oncotarget* **5**, 1458–1474 (2014).
32. Y. C. Lee *et al.*, Inhibition of cell adhesion by a cadherin-11 antibody thwarts bone metastasis. *Mol. Cancer Res.* **11**, 1401–1411 (2013).
33. V. Padmanaban *et al.*, E-cadherin is required for metastasis in multiple models of breast cancer. *Nature* **573**, 439–444 (2019).
34. N. M. Aiello *et al.*, EMT subtype influences epithelial plasticity and mode of cell migration. *Dev. Cell* **45**, 681–695.e4 (2018).
35. P. P. Sfikakis, N. I. Vlachogiannis, P. F. Christopoulos, Cadherin-11 as a therapeutic target in chronic, inflammatory rheumatic diseases. *Clin. Immunol.* **176**, 107–113 (2017).
36. E. Piskounova *et al.*, Oxidative stress inhibits distant metastasis by human melanoma cells. *Nature* **527**, 186–191 (2015).

37. X. Hong *et al.*, The lipogenic regulator SREBP2 induces transferrin in circulating melanoma cells and suppresses ferroptosis. *Cancer Discov.* **11**, 678–695 (2021).
38. V. Murlidhar *et al.*, Poor prognosis indicated by venous circulating tumor cell clusters in early-stage lung cancers. *Cancer Res.* **77**, 5194–5206 (2017).
39. A. Roy, A. Kucukural, Y. Zhang, I-TASSER: A unified platform for automated protein structure and function prediction. *Nat. Protoc.* **5**, 725–738 (2010).
40. A. Roy, J. Yang, Y. Zhang, COFACTOR: An accurate comparative algorithm for structure-based protein function annotation. *Nucleic Acids Res.* **40**, W471–W477 (2012).
41. M. Torchala, P. A. Bates, Predicting the structure of protein-protein complexes using the SwarmDock Web Server. *Methods Mol. Biol.* **1137**, 181–197 (2014).
42. R. L. Porter *et al.*, Epithelial to mesenchymal plasticity and differential response to therapies in pancreatic ductal adenocarcinoma. *Proc. Natl. Acad. Sci. U.S.A.* **116**, 26835–26845 (2019).
43. J. F. Edd *et al.*, Microfluidic concentration and separation of circulating tumor cell clusters from large blood volumes. *Lab Chip* **20**, 558–567 (2020).
44. M. Ghandi *et al.*, CCLE Dataset. https://sites.broadinstitute.org/ccle/datasets. Accessed 15 October 2021.
45. M. Uhlen *et al.*, A genome-wide transcriptomic analysis of protein-coding genes in human blood cells. RNA HPA blood cell gene data The Human Protein Atlas. https://www.proteinatlas.org/about/download. Accessed 2 February 2022.